

Groupwise Spectral Log-Demons Framework for Atlas Construction

Herve Lombaert^{1,2}, Leo Grady³, Xavier Pennec²,
Jean-Marc Peyrat⁴, Nicholas Ayache², Farida Cheriet¹

¹ Ecole Polytechnique de Montreal, Canada

² INRIA Sophia Antipolis, France

³ Siemens Corporate Research, Princeton, NJ

⁴ Siemens Molecular Imaging, Oxford, UK

Abstract. We introduce a new framework to construct atlases from images with very large and complex deformations. The atlas is build in parallel with groupwise registrations by extending the symmetric Log-Demons algorithm. We describe and evaluate two forms of our framework: the *Groupwise Log-Demons* (GL-Demons) is faster but is limited to local nonrigid deformations, and the *Groupwise Spectral Log-Demons* (GSL-Demons) is slower but, due to isometry-invariant representations of images, can construct atlases of organs with high shape variability. We demonstrate our framework by constructing atlases from hearts with high shape variability.

1 Introduction

Statistics on complex characteristics with high anatomical and functional variability require the normalization of measurements across subjects to establish a population average and deviations from that average. The process of shape averaging [22,5,27] becomes particularly complex, and still remains unsolved, with organs undergoing large shape disparities. In the present state-of-the-art, the concept of geodesic shape averaging allows unbiased constructions of atlases through diffeomorphic methods [12,2,17], i.e., the transformation of a reference shape toward an average (the geometry of the atlas) follows a geodesic path on a Riemannian manifold (the space of diffeomorphic transformations). While the LDDMM [4,3,6] or forward scheme approaches [1,8] provide elegant mathematical frameworks for averaging shapes, these methods could be slow and find their limitations with high shape variability. Guimond *et al.* [10] proposed a fast and efficient algorithm [19,16,26] with sequential (pairwise) registrations to a reference image. A new simultaneous (groupwise) registration approach would enable the construction of an atlas in parallel, during the registration process (rather than with a series of pairwise registrations). To do so, *firstly*, we extend the symmetric Demons algorithm [25] to perform a groupwise registration of a set of images in order to construct their atlas. However, as in most registration methods, transformation updates based on the image gradients are inherently limited by their local scope. *Secondly*, we introduce a new update scheme for groupwise registration based on the spectral decomposition of graph Laplacians [7,23,13], that is invariant to shape isometry and is capable of capturing large deformations during the construction of the atlas. We provide *two forms* of our groupwise registration framework that we name the *Groupwise Log-Demons* (**GL-Demons**, faster and suited for local nonrigid

deformations), and the *Groupwise Spectral Log-Demons* (**GSL-Demons**, slower but capable of capturing very large deformations). We evaluate the two forms of our new framework by constructing atlases of images with very large deformations.

2 Method

The atlas is defined as the set of N images $\{I_i\}_{i=1..N}$ nonrigidly aligned to their average shape \tilde{I} . Our new shape averaging framework extends the symmetric Log-Demons algorithm [25] and can use classical gradient-based updates (*GL-Demons*) or an improved spectral matching for groupwise registration (*GSL-Demons*). We begin by briefly reviewing each component.

2.1 Diffeomorphic Registration

A diffeomorphic transformation ϕ between two images (such that $F(\cdot) \mapsto M(\phi(\cdot))$ or simply $F \mapsto M \circ \phi$) guarantees a smooth one-to-one mapping (i.e., differentiable and invertible, without creating foldings in space). From the theory of Lie groups, the exponential map of a stationary velocity field v generates a diffeomorphic transformation $\phi = \exp(v)$ (approximated with the scaling-and-squaring method [24]). The Log-Demons algorithm alternates the optimization of a similarity term and a regularization term by decoupling them with a hidden variable (the correspondence c). The algorithm is slightly modified from [25] to converge toward an average shape by minimizing the following energy (controlled with $\alpha_i, \alpha_x, \alpha_T$):

$$E(F, M, c, v) = \alpha_i^2 \text{Sim}(F', M') + \alpha_x^2 \text{dist}(c, v)^2 + \alpha_T^2 \text{Reg}(v), \text{ where} \quad (1)$$

$$\text{Sim}(F', M') = (F' - M')^2, \text{ dist}(c, v) = \|c - v\|, \text{ and } \text{Reg}(v) = \|\nabla v\|^2$$

The similarity term incorporates diffeomorphism and symmetry with $F' = F \circ \exp(-c)$ and $M' = M \circ \exp(+c)$. Both images F' and M' effectively converge toward an average shape $\tilde{I} = F \circ \phi^{-1} + M \circ \phi$ (similar to the approaches in [2,6]).

2.2 Spectral Correspondence

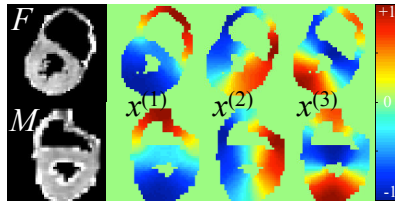
The computation of the velocity field updates in the Log-Demons is inherently limited by the local scope of the update forces derived from the image gradient, i.e., it requires texture data which is generally local information. We now describe a new update scheme based on spectral correspondence [21,11,18,14,13] that will enable the construction of atlases with large deformations. Let us first consider I_Ω , the portion of an image I bounded by a contour Ω . We build a connected graph $\mathcal{G} = (\mathcal{V}, \mathcal{E})$ where the vertices \mathcal{V} represent the pixels of I_Ω and the edges \mathcal{E} define the neighborhood structure within I_Ω . The corresponding adjacency matrix W [9] represents the edge weights ($W_{ij} = w_{ij}$ if pixels (i, j) are neighbors, 0 otherwise), such that pixels with similar intensity and close in space would have strong links in \mathcal{G} (e.g., $w_{ij} = \exp(-\beta(I(i) - I(j))^2) / \|\mathbf{x}(i) - \mathbf{x}(j)\|^2$ where \mathbf{x} are Euclidean coordinates and β a parameter). The Laplacian operator on a graph [9] is formulated as a $|\mathcal{V}| \times |\mathcal{V}|$ matrix with the form $\mathcal{L} = D^{-1}(D - W)$, where D is the (diagonal) degree matrix containing the node degrees $D_{ii} = \sum_j W_{ij}$.

Spectral Coordinates The decomposition of the Laplacian matrix $\mathcal{L} = \mathcal{X}^T \Lambda \mathcal{X}$ reveals the graph spectrum [7] which comprises the eigenvalues $\Lambda = \text{diag}(\lambda_0, \lambda_1, \dots, \lambda_{|\mathcal{V}|})$ (in increasing order) and their associated eigenmodes $\mathcal{X} = (\mathcal{x}^{(0)}, \mathcal{x}^{(1)}, \dots, \mathcal{x}^{(|\mathcal{V}|)})$ (a $|\mathcal{V}| \times |\mathcal{V}|$ matrix where columns $\mathcal{x}^{(\cdot)}$ are eigenmodes). The first eigenmode is trivial ($\lambda_0 = 0$) and the following non-trivial eigenmodes are the fundamental modes of vibrations of a shape depicted by I_Ω . The eigenmodes associated with the first k smallest non-zero eigenvalues (the lower frequencies) represent the k -dimensional *spectral coordinates* (each point $i \in I_\Omega$ has the coordinates $\mathcal{x}(i) = (\mathcal{x}^{(1)}(i), \mathcal{x}^{(2)}(i), \dots, \mathcal{x}^{(k)}(i))$ defined in a spectral domain). These lowest modes of vibration have the strong property of being smooth and invariant to shape isometry (i.e., shapes in different poses would share the same spectral coordinates at each point, see *below*).

However, the eigenmodes need to be rearranged as a result of sign ambiguity ($\mathcal{x}^{(\cdot)}$ and $-\mathcal{x}^{(\cdot)}$ are both valid eigenmodes), algebraic multiplicity (many eigenmodes can share the same eigenvalue), and imperfection in isometry (changing the multiplicity and ordering of the eigenvalues). Firstly, their values are scaled to fit the range $[-1; +1]$, i.e., for negative values:

$\mathcal{x}^{(\cdot)-} \leftarrow \mathcal{x}^{(\cdot)-} / \min\{\mathcal{x}^{(\cdot)-}\}$ and for positive values: $\mathcal{x}^{(\cdot)+} \leftarrow \mathcal{x}^{(\cdot)+} / \max\{\mathcal{x}^{(\cdot)+}\}$.

Secondly, the eigenmodes of two images, \mathcal{X}_F and \mathcal{X}_M , are reordered with the optimal permutation π (where $\mathcal{x}_F^{(\cdot)} \mapsto \mathcal{x}_M^{\pi(\cdot)}$) which may be found with the Hungarian algorithm that minimizes the following dissimilarity matrix:



Three lowest frequency eigenmodes of two images

$$C(u, v) = \sqrt{\frac{1}{|I_\Omega|} \sum_{i \in I_\Omega} \left(\mathcal{x}_F^{(u)}(i) - \mathcal{x}_M^{(v)}(i) \right)^2} + \sqrt{\sum_{i, j} \left(h_F^{\mathcal{x}^{(u)}}(i, j) - h_M^{\mathcal{x}^{(v)}}(i, j) \right)^2} \quad (2)$$

The first term is the difference in spectral coordinates between the images. The second term measures the dissimilarities between the joint histograms $h(i, j)$ (a 2D matrix where the element (i, j) is the joint probability of having at the same time the intensity i and the eigenmodal value $\mathcal{x}^{(\cdot)} = j$). The sign ambiguity can be removed by optimizing, instead, the dissimilarity matrix $Q(u, v) = \min\{C(u, v), C(u, -v)\}$. To keep the notation simple in the next sections, we assume the spectral coordinates have been appropriately signed, scaled and reordered using this method.

Spectral Matching The correspondence between two images F and M is established (Alg. (1)) by finding the nearest neighbors in the spectral domain (e.g., with fast k -d trees). Put differently, if $\mathcal{x}_F(i)$ is the closest point to $\mathcal{x}_M(j)$ then the pixel i corresponds with j . This simple nearest-neighbor scheme is extended to add similarity constraints on intensity and space by adding image intensities and Euclidean coordinates to the spectral embedding: $\mathbf{X} = (\alpha_i I, \alpha_s \mathbf{x}, \alpha_g \mathcal{X})$. Nearest points between \mathbf{X}_F and \mathbf{X}_M actually locate the best compromise among three strong properties: points with similar isometric (or geometric) properties, similar image intensities, and similar location (each weighted with $\alpha_{g, i, s}$). To be more precise, this corresponds to minimizing the energy $E(F, M, \phi) = \text{Sim}(F, M)$ where the regularization (similarly

Algorithm 1 Spectral Correspondence**Input:** Images F, M .**Output:** Correspondence c mapping F to M

- Compute general Laplacians $\mathcal{L}_F, \mathcal{L}_M$.
- $\mathcal{L} = D^{-1}(D - W)$, where
 $W_{ij} = \exp(-\beta(I(i) - I(j))^2) / \|\mathbf{x}(i) - \mathbf{x}(j)\|^2$
 $D_{ii} = \sum_j W_{ij}$,
- Compute first k eigenmodes of Laplacians
- Reorder \mathcal{X}_M with respect to \mathcal{X}_F (Eq. (2))
- Build embeddings:
 $\mathbf{F} = (I_F, \mathbf{x}_F, \mathcal{X}_F)$; $\mathbf{M} = (I_M, \mathbf{x}_M, \mathcal{X}_M)$
- Find c mapping nearest points $\mathbf{F} \mapsto \mathbf{M}$

Algorithm 2 Groupwise Demons Framework**Input:** N images with initial reference (e.g., $\tilde{I} = I_1$)**Output:** Transformations $\phi_i = \exp(v_i)$ mapping \tilde{I} to I_i
Average shape is $\tilde{I} = \frac{1}{N} \sum_{i=1}^N I_i \circ \exp(v_i)$ **repeat****for** $i = 1 \rightarrow N$ **do**

- Find updates $u_i \leftarrow \text{mapping}(\tilde{I}, I_i \circ \exp(v_i))$.
(mapping() differs in GL and GSL-Demons)
 - Smooth updates: $u_i \leftarrow K_{\text{fluid}} * u_i$.
(convolution of a Gaussian kernel on u_i)
 - Update velocity fields: $v_i \leftarrow \log(\exp(v_i) \circ \exp(u_i))$
(approximated with $v_i \leftarrow v_i + u_i$).
 - Smooth velocity fields: $v_i \leftarrow K_{\text{diff}} * v_i$.
- end for**
- Get reference update: $u_{\text{ref}} = -\frac{1}{N} \sum_{i=1}^N v_i$
 - Update velocity fields: $v_i \leftarrow v_i + u_{\text{ref}}$.
 - Update reference: $\tilde{I} \leftarrow \frac{1}{N} \sum_{i=1}^N I_i \circ \exp(v_i)$.
- until** convergence

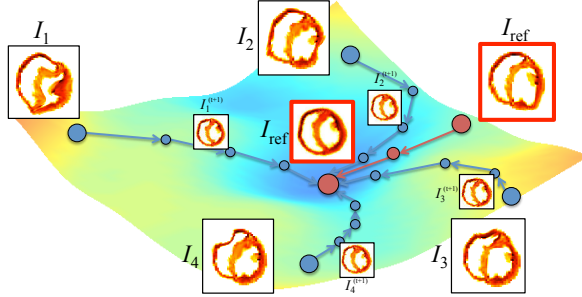


Fig. 1. Groupwise Demons: Simultaneous registration of 4 images (blue circles) toward a reference image that evolves in the space of diffeomorphisms (colored manifold). The reference image is computed in parallel and converges to the average shape (middle red circle).

to [14]) is enforced with the smoothness of the spectral and spatial components:

$$\text{Sim}(F, M) = (F - M \circ \phi)^2 + \frac{\alpha_s^2}{\alpha_f^2} (\mathbf{x}_F - \mathbf{x}_{M \circ \phi})^2 + \frac{\alpha_g^2}{\alpha_f^2} (\mathcal{X}_F - \mathcal{X}_{M \circ \phi})^2, \quad (3)$$

where \mathcal{X}_F and $\mathcal{X}_{M \circ \phi}$ are the spectral coordinates of corresponding points. This matching technique that is invariant to isometry will enable the capture of large deformations for our atlas construction.

2.3 Groupwise Demons Framework

Our framework is based on Guimond's *et al.* approach [10] where they construct the average image \tilde{I} *sequentially* by alternating between pairwise registrations (fixing a reference image) and updates of the average image (transforming the reference image). Our novelty is to directly compute \tilde{I} *in parallel* with simultaneous (groupwise) registrations (illustrated in Fig. 1). To do so, Eq. (1) is extended to incorporate N velocity fields that warp all images $\{I_i \circ \exp(c_i)\}$ toward the average image \tilde{I} . The new groupwise framework is summarized in Alg. (2) and the underlying energy is:

$$E(\tilde{I}, \{I_i, c_i, v_i\}) = \frac{1}{N} \sum_{i=1}^N \left(\alpha_s^2 \text{Sim}(\tilde{I}, I_i \circ \exp(c_i)) + \alpha_x^2 \text{dist}(c_i, v_i)^2 + \alpha_T^2 \text{Reg}(v_i) \right) \quad (4)$$

The reference image can be optionally generated with weighted contributions from all images (e.g., weights different than $1/N$ in order to remove outliers). The minimization of all similarity terms, $\{\text{Sim}(I, I'_i)\}$, causes all warped images to become similar to the reference image and the sum of all velocity fields is brought to a minimal value at convergence. Similar to the convergence of [10], the Groupwise Demons framework effectively brings the reference image toward the barycenter of all images. The average image is simply generated with $\tilde{I} = \frac{1}{N} \sum_{i=1}^N I_i \circ \exp(c_i)$.

Groupwise Spectral Log-Demons The update schemes based on image gradients and on spectral correspondence can be used in the Groupwise Demons framework. The *Groupwise Log-Demons* (GL-Demons) algorithm uses update forces derived from the image gradient and is well suited for images with local nonrigid deformations, while the *Groupwise Spectral Log-Demons* (GSL-Demons) algorithm uses spectral correspondences as update forces (i.e., u is found with Alg. (1)) and is better suited for large and highly non-local deformations. GSL-Demons enables large jumps during the construction of the atlas where points move toward their isometric equivalents even if they are far away in space. The atlas construction can handle very large deformations and convergences in fewer iterations (typically 5 iterations are sufficient). The energy has the same form of Eq. (4) and uses the similarity term of Eq. (3).

Multilevel Scheme Moreover, large and complex deformations can be captured in a low resolution level with *GSL-Demons*, improving thus the processing time, while the remaining small and local deformations can be recovered with *GL-Demons* in higher resolutions. This multilevel approach keeps the computation of the eigenmodes tractable.

3 Results

GL-Demons and *GSL-Demons* are evaluated by constructing atlases of images with large deformations. In the synthetic experiment, we verify convergence toward an average shape, and the handling of highly complex deformations (parameters: $\sigma_{\text{fluid,diff}} = 1, \alpha_x = 1, k = 5, \alpha_g = 0.1, \alpha_s = 0.2, \alpha_i = 0.7$ in 2D). In a second experiment, we use both algorithms with real cardiac images that exhibit high shape variability (parameters: $\sigma_{\text{fluid,diff}} = 0.75, \alpha_x = 1, k = 5, \alpha_g = 0.25, \alpha_s = 0.35, \alpha_i = 0.4$ in 3D).

Synthetic deformations Convergence and capture of large deformations are now evaluated. $N/2$ velocity fields v are generated randomly using 15 control points with random locations in the image and random displacements of at most 15 pixels (20% of the image size) that are diffused over the image. Their forward and background transformations ($\exp(v)$ and $\exp(-v)$) are applied to an initial image I_0 , holding thus the average shape to I_0 (establishing our ground truth). Since we compare the convergence and its rate, and not the final performance, the multi-level scheme (which should be used in real applications) is not applied. Fig. 2 shows the groupwise registrations of 10 random hearts (2D 75×75 images) through 100 trials (a total of 1000 hearts). The average Dice metric (measuring the overlap) between all computed average shapes and I_0 as well as the intensity errors (MSE) reveal that the reference shape (defined arbitrarily as one of the 10 images) evolves toward the ground truth (i.e., Dice increases and MSE decreases). Moreover, the N deformation fields

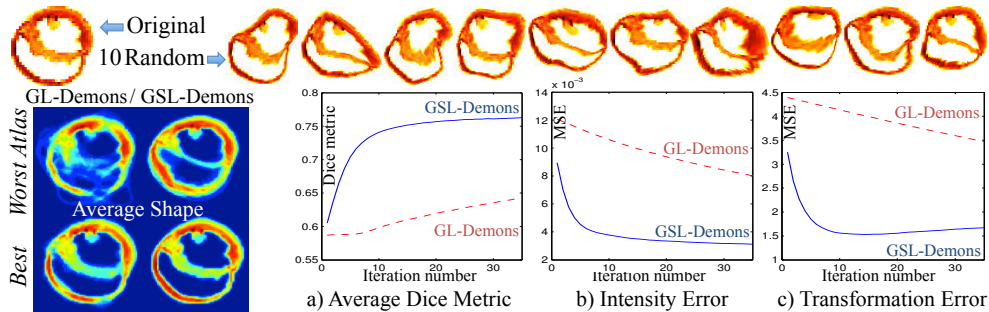


Fig. 2. Groupwise registration of 10 images deformed randomly (100 trials, 1 sample on top row, with known ground truth) using *GL-Demons* and *GSL-Demons*, *Left*) Best and worst atlases (based on Dice metric among 100 trials) demonstrating the capability of the *GSL-Demons* to handle large deformations, *a*) Average Dice metric with ground truth, *b*) Intensity difference between average shape and ground truth, *c*) transformation error with ground truth. *GSL-Demons* converges faster toward the average shape.

become closer to the ground truth during registration. The striking difference in the convergence rates shows the full power of *GSL-Demons* (less than 5 iterations are required) while *GL-Demons* might not converge with such large deformations (we stopped the algorithms after 200 iterations). Time-wise, 35 iterations takes 194 seconds with *GSL-Demons*, and 53 seconds with *GL-Demons* (using unoptimized Matlab code on a 2.53GHz Core 2 Duo). *GSL-Demons* shows a better performance with high deformations than *GL-Demons*.

Cardiac Atlases We now evaluate the construction of atlases with organs of high shape variability. *Ex vivo* hearts are particularly challenging to register as they present a high variability in fixture poses due to flabby ventricular walls. The human *ex vivo* DTMRI dataset [20,16,15] provides good candidates to evaluate our algorithms. We use four hearts ($b = 0$ images of size 64^3) that were excluded in the construction of the human atlas [15] due to their hypertrophy and highly deformed shapes (see Fig. 3). *GL-Demons* (with 4 resolution levels) fail in recovering the shapes of the right ventricles, while *GSL-Demons* successfully constructs the atlas even with 1 level of resolution (downsampled images at size 28^3). As a comparison, 35 iterations takes 40 minutes in Matlab with *GSL-Demons* and 9 minutes with *GL-Demons*. Using *GSL-Demons* with 4 resolution levels reduce the intensity error (MSE) by half (from 10.8 to 5.08). Moreover, the Jacobian determinants of the transformation fields show that the large and highly non-local deformations are successfully captured with the spectral-based update scheme (high and smooth Jacobian in Fig. 3 b) while local deformations are captured with the gradient-based update scheme in the higher levels of *GSL-Demons* (Fig. 3 c).

4 Conclusion

We addressed the problem of atlas construction that is limited by large deformations between images. We proposed a new framework with two forms to construct an atlas

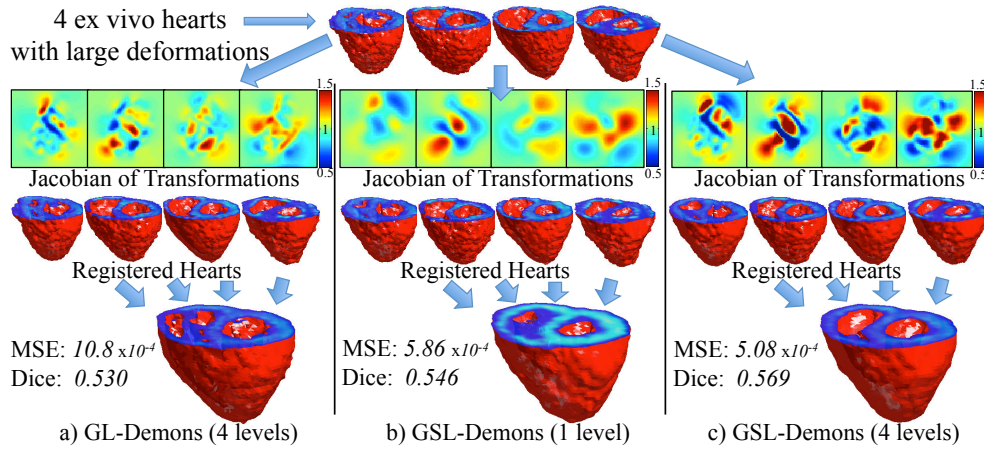


Fig. 3. Atlas of *ex vivo* hearts (isosurfaces are shown) using a) *GL-Demons* (4 levels, showing failure in the right ventricle), b) *GSL-Demons* (1 level), c) and *GSL-Demons* (4 levels, with correct right ventricle). *GSL-Demons* capture successfully large deformations. Jacobian determinants (axial planes) show that spectral matching capture smooth and large deformations while gradient-based updates capture local deformations.

in parallel with groupwise registrations: *GL-Demons* is faster but is limited by its gradient-based forces, while *GSL-Demons* is slower but can capture very large deformations due to its spectral components. We evaluated our framework by constructing atlases from images with complex deformations. Results showed convergence to an average shape and atlases were successfully created under large deformations of 20% of the image size using 1000 random hearts. We additionally showed that *GSL-Demons* can construct an atlas for a challenging dataset of *ex vivo* hearts with high shape variability. Future work will focus on implementation (converting the Matlab code, also, the groupwise nature of our framework could highly benefit from parallel computing, e.g., GPU) and improving the computation time of the spectral decomposition (e.g., reuse of pre-computations, approximations). Nevertheless, our current framework enables the construction of atlases from images with very large and complex deformations.

Acknowledgements The authors wish to thank Pierre Croisille for *ex vivo* hearts as well as Hervé Delingette for helpful comments. The project was supported financially by the National Science and Engineering Research Council of Canada (NSERC).

References

1. S. Allasonnière, Y. Amit, and A. Trouvé. Towards a coherent statistical framework for dense deformable template estimation. *J. Royal Stat. Soc.*, 69:3–29, 2007.¹
2. B. Avants and J. C. Gee. Geodesic estimation for large deformation anatomical shape averaging and interpolation. *NeuroImage*, 23:139–150, 2004.^{1, 2}
3. M. F. Beg and A. Khan. Computing an average anatomical atlas using LDDMM and geodesic shooting. In *ISBI*, pages 1116–1119, 2006.¹

4. M. F. Beg, M. I. Miller, A. Trouvé, and L. Younes. Computing large deformation metric mappings via geodesic flows of diffeomorphisms. *IJCV*, 61:139–157, 2005.¹
5. K. K. Bhatia, J. V. Hajnal, B. K. Puri, A. D. Edwards, and D. Rueckert. Consistent groupwise non-rigid registration for atlas construction. In *ISBI*, pages 908–911, 2004.¹
6. M. Bossa, M. Hernandez, and S. Olmos. Contributions to 3D diffeomorphic atlas estimation: application to brain images. In *MICCAI*, pages 667–674, 2007.^{1, 2}
7. F. Chung. *Spectral Graph Theory*. AMS, 1997.^{1, 3}
8. S. Durrleman, P. Fillard, X. Pennec, A. Trouvé, and N. Ayache. Registration, atlas estimation and variability analysis of white matter fiber bundles modeled as currents. *NeuroImage*, 55:1073–1090, 2011.¹
9. L. Grady and J. R. Polimeni. *Discrete Calculus: Applied Analysis on Graphs for Computational Science*. Springer, 2010.²
10. A. Guimond, J. Meunier, and J. P. Thirion. Average brain models: a convergence study. *Computer Vision and Image Understanding*, pages 192–210, 2000.^{1, 4, 5}
11. V. Jain and H. Zhang. Robust 3D shape correspondence in the spectral domain. In *Int. Conf. on Shape Modeling and App.*, page 19, 2006.²
12. S. Joshi, B. Davis, M. Jomier, and G. Gerig. Unbiased diffeomorphic atlas construction for computational anatomy. *NeuroImage*, 23:151–160, 2004.¹
13. H. Lombaert, L. Grady, X. Pennec, N. Ayache, and F. Chieriet. Spectral Demons - Image Registration via Global Spectral Correspondence. In *ECCV*, 2012.^{1, 2}
14. H. Lombaert, L. Grady, J. R. Polimeni, and F. Chieriet. Fast brain matching with spectral correspondence. In *IPMI*, pages 660–670, 2011.^{2, 4}
15. H. Lombaert, J.-M. Peyrat, P. Croisille, S. Rapacchi, L. Fanton, F. Chieriet, P. Clarysse, I. Magnin, H. Delingette, and N. Ayache. Human atlas of the cardiac fiber architecture: Study on a healthy population. *IEEE Trans. on Med. Imaging*, 31:1436–1447, 2012.⁶
16. H. Lombaert, J.-M. Peyrat, P. Croisille, S. Rapacchi, L. Fanton, P. Clarysse, H. Delingette, and N. Ayache. Statistical analysis of the human cardiac fiber architecture from DT-MRI. In *FIMH*, volume 6666, pages 171–179, 2011.^{1, 6}
17. S. Marsland, C. J. Twining, and C. J. Taylor. Groupwise non-rigid registration using polyharmonic Clamped-Plate splines. In *MICCAI*, volume 2879, pages 771–779, 2003.¹
18. D. Mateus, R. Horaud, D. Knossow, F. Cuzzolin, and E. Boyer. Articulated shape matching using Laplacian eigenfunctions and unsupervised point registration. In *CVPR*, pages 1–8, 2008.²
19. J.-M. Peyrat, M. Sermesant, X. Pennec, H. Delingette, C. Xu, E. R. McVeigh, and N. Ayache. A computational framework for the statistical analysis of cardiac diffusion tensors: application to a small database of canine hearts. *IEEE Trans. on Med. Imaging*, 26(11):1500–1514, 2007.¹
20. S. Rapacchi, P. Croisille, V. Pai, D. Grenier, M. Viallon, P. Kellman, N. Mewton, and H. Wen. Reducing motion sensitivity in free breathing DWI of the heart with localized Principal Component Analysis. In *ISMRM*, 2010.⁶
21. L. S. Shapiro and J. M. Brady. Feature-based correspondence: an eigenvector approach. *Image and Vision Computing*, 10:283–288, 1992.²
22. C. Studholme and V. Cardenas. A template free approach to volumetric spatial normalization of brain anatomy. *Pattern Recogn. Lett.*, 25:1191–1202, 2004.¹
23. O. van Kaick, H. Zhang, G. Hamarneh, and D. Cohen-Or. A survey on shape correspondence. *Eurographics*, 30(6):1681–1707, 2011.¹
24. T. Vercauteren, X. Pennec, A. Perchant, and N. Ayache. Non-parametric diffeomorphic image registration with the demons algorithm. In *MICCAI*, pages 319–326, 2007.²
25. T. Vercauteren, X. Pennec, A. Perchant, and N. Ayache. Symmetric Log-domain diffeomorphic registration: a demons-based approach. In *MICCAI*, 2008.^{1, 2}
26. G. Wu, H. Jia, Q. Wang, and D. Shen. SharpMean: groupwise registration guided by sharp mean image and tree-based registration. *NeuroImage*, 56(4):1968–1981, 2011.¹
27. L. Zollei, Learned E. Miller, W. E. L. Grimson, and wells W. M. Iii. Efficient population registration of 3D data. In *ICCV 2005, Computer Vision for Biomedical Image Applications*, 2005.¹